ADVANCED MATERIALS
www.advmat.de

Single Crystal Formamidinium Lead Iodide ($FAPbI_3$): Insight into the Structural, Optical, and Electrical Properties

Qifeng Han, Sang-Hoon Bae, Pengyu Sun, Yao-Tsung Hsieh, Yang (Michael) Yang, You Seung Rim, Hongxiang Zhao, Qi Chen, Wangzhou Shi, Gang Li, and Yang Yang**

Recently, hybrid organolead trihalide perovskite (OTP) solar cells have developed as a promising candidate in photovoltaics due to their excellent properties including a direct bandgap,[1] strong absorption coefficient,[2] long carrier lifetime,[3] and high mobility.[4,5] Basically, the OTP structure is ABX_3 where A and B represent an organic ammonium cation and Pb, respectively, and X is a halide such as I or a combination of Cl, Br, and I.[6–12] Among these candidates for solar cell application, the most popular is methylammonium ($CH_3NH_3^+$ or MA) lead iodide ($MAPbI_3$), reaching nearly 20% power conversion efficiency.[13,14] Most recently, formamidinium ($NH_2CH{=}NH_2^+$ or FA) lead iodide ($FAPbI_3$) has attracted significant attention due to several advantages: (1) the larger organic FA cation can replace the MA cation and form a more symmetric crystal structure, (2) the smaller bandgap of $FAPbI_3$ allows for near infrared absorption, and (3) $FAPbI_3$ has an elevated decomposition temperature and thus potential to improve stability.[15–18] Perovskite solar cells incorporating $FAPbI_3$ in absorber layer ($(FAPbI_3)_{0.85}(MAPbBr_3)_{0.15}$) have achieved record certified power conversion efficiency of 20.1%.[19] Despite of many studies on FA-based perovskite structures in thin film solar cells, the intrinsic electrical, optical, and structural properties of $FAPbI_3$ still require further study.[20,21] Typically, it is difficult to understand the fundamental properties of $FAPbI_3$ in thin films due to a favorable phase transforming at room temperature and the large amount of recombination sites due to grain boundaries, voids, and surface defects. Single crystals, on the other hand, provide an excellent model system to study the intrinsic electrical and optical properties of these materials due to their high purity. This is particularly important to understand the limits of these materials. So far, several approaches of the single crystal growth of $MAPbI_3$ and $MAPbBr_3$ have been studied. Huang and co-workers reported a 10 mm sized growth of single crystal $MAPbI_3$ using a top-seeded solution method with a temperature gradient and obtained a carrier diffusion length over 175 μm.[22] Bakr and co-workers reported an antisolvent vapor-assisted crystallization approach that enabled sizable crack-free $MAPbX_3$ (X = I or Br) single crystals with volumes exceeding 100 mm^3.[23] In addition, Tao and co-workers and Lin and co-workers used a cooling solution method to grow $MAPbI_3$ single crystals in HI solution.[24,25] Later Bakr and co-workers and Liu et al. separately reported using an inverse temperature crystallization method to grow $MAPbX_3$ perovskite single crystals.[26,27] Single crystal $FAPbI_3$ has hardly been reported. Kanatzidis and co-workers reported the fundamental study of 50 μm sized single crystal $FAPbI_3$, which is significantly smaller than the 10 mm size $MAPbI_3$.[28] Bakr and co-workers also grew $FAPbX_3$ single crystals using the similar methods as they grew $MAPbX_3$ single crystals.[29]

Here, we demonstrate for the first time the growth of 5 mm sized single crystal $FAPbI_3$. The crystal was grown using a modified inverse temperature crystallization method. We used a cooling solution method to first grow the $FAPbI_3$ seed crystal, followed by placing the seed crystals in an inverse temperature crystallization precursor to obtain larger crystals. The thermal, optical, and electrical properties of single crystal $FAPbI_3$ were explored. In addition, we fabricated single crystal $FAPbI_3$ photodetectors and investigated photoconductivity and photoresponse. Low noise current and high switching speeds were confirmed.

$MAPbI_3$ has a stable perovskite phase during growth at the temperature range from 60 to 110 °C for various growth methods. However, a small growth temperature variation could affect the growth process in the case of $FAPbI_3$. In order to obtain a $FAPbI_3$ seed crystal, we first attempted the inverse temperature crystallization method. Homogenous nucleations of α-phase $FAPbI_3$ started after 15 min at 100 °C. The crystal growth speed was subsequently enhanced, leading to thermal fluctuation particularly at the solution/air interface as a result of the endothermic reaction. Light yellow δ-phase $FAPbI_3$ and some needle like NH_4PbI_3 appeared at this time impeded the α-phase crystal growth.[29,30] Therefore, it is difficult to obtain high quality single crystal $FAPbI_3$ seeds directly using the inverse temperature crystallization method. In order to minimize the side effects, we use a new process combining the cooling solution and inverse temperature crystallization methods to grow single crystal $FAPbI_3$. First, we used the

Dr. Q. Han, S.-H. Bae, P. Sun, Y.-T. Hsieh, Dr. Y. (Michael) Yang, Dr. Y. S. Rim, H. Zhao, Dr. Q. Chen, Dr. G. Li, Prof. Y. Yang
Department of Materials Science and Engineering
University of California Los Angeles
Los Angeles, CA 90095, USA
E-mail: gangl@ucla.edu; yangy@ucla.edu
Dr. Q. Han, S.-H. Bae, Y.-T. Hsieh, H. Zhao, Dr. Q. Chen, Prof. Y. Yang
California NanoSystems Institute
University of California Los Angeles
Los Angeles, CA 90095, USA
Dr. Q. Han, Prof. W. Shi
Department of Physics
Shanghai Normal University
Shanghai 200234, China

DOI: 10.1002/adma.201505002

cooling solution method to grow single crystals seeds. Lead (II) acetate trihydrate (Pb $(ac)_2 \cdot 3H_2O$) and fomamidine acetate salt (FAac) first dissolved in HI at 105 °C and then gradually cooled to 70 °C. The seed crystals were obtained after 6 h. The details could be found in the Experimental Section. By placing a few seed crystals into the inverse temperature crystallization precursor solution and keeping it at 100 °C, the seed crystal grew larger. This heterogeneous nucleation process effectively reduced NH_4PbI_3 and δ-phase $FAPbI_3$ growth comparing to homogeneous nucleation, which is attributed to a small number of nucleation centers that reduce the precipitation rate and could decrease temperature fluctuation within the solution. In addition, we gradually raised the temperature from 100 to 105 °C after crystals began to grow. This compensated for the heat loss caused by crystal growth. After 1 h, the growth speed gradually decreased, and we turned back the temperature to 100 °C to grow the crystal. By repeating the inverse temperature crystallization process three times, a large $FAPbI_3$ single crystal was synthesized.

Interestingly, the color of $FAPbI_3$ gradually changed from black (**Figure 1**a) to yellow (Figure 1b) after 10 d, regardless of storage in vacuum or inert gas. The inset of Figure 1 showed the photos of the same 5 mm size single crystal $FAPbI_3$ before and after the phase change at room temperature. The yellow colored crystal could also rapidly recover back to the black color without any visible shape change after the annealing at 185 °C for only 2 min as shown in Figure S1 (Supporting Information). This change of single crystal $FAPbI_3$ was monitored by heating a small yellow crystal from room temperature to 550 °C at the rate of 5 °C min^{-1} in Ar atmosphere using thermogravimetric analysis and differential scanning calorimetry (TGA-DSC) (Figure 1c). An endothermic peak was observed at 185 °C without mass loss, corresponding to the color change related to the phase transformation of the single crystal $FAPbI_3$. A mass loss (over 20%), associated with the strong exothermic peak, occurred at 320–360 °C and is related to the decomposition of hydrogen iodide (HI).[27] From the temperatures of 375–420 °C, a mass loss (≈6%) occurred. This could be attributed to the decomposition of the formamidinium. This means that the formamidinium is more stable than iodide ion in $FAPbI_3$ single crystal. The decomposition temperature of the $FAPbI_3$ single crystal is higher than $MAPbI_3$ single crystal,[27] which indicates that the thermal stability of $FAPbI_3$ is better than $MAPbI_3$.

In order to understand the differences between the black and yellow crystals, X-ray diffraction (XRD) was performed on ground black and yellow single crystals to identify phase change. The results are shown in Figure 1d,e. For the black single crystal, all peaks were indexed to a trigonal perovskite phase ($P3m1$ space group, α-phase) with $a = b = 0.898$ nm and $c = 1.101$ nm. On the other hand, the yellow crystal showed the hexagonal system ($P6_3mc$ space group, δ-phase) with $a = b = 0.866$ nm and $c = 0.790$ nm.[28] The two phases were also studied by Raman spectroscopy (Figure S2, Supporting Information) using a 514.5 nm laser, where the main Raman peak redshifted from 135 to 111 cm^{-1} while the $FAPbI_3$ single crystal changed from α-phase to δ-phase, which might be related to the vibration of FA molecule.[31,32]

The photoluminescence (PL) properties of $FAPbI_3$ were measured at room temperature using a red light source at

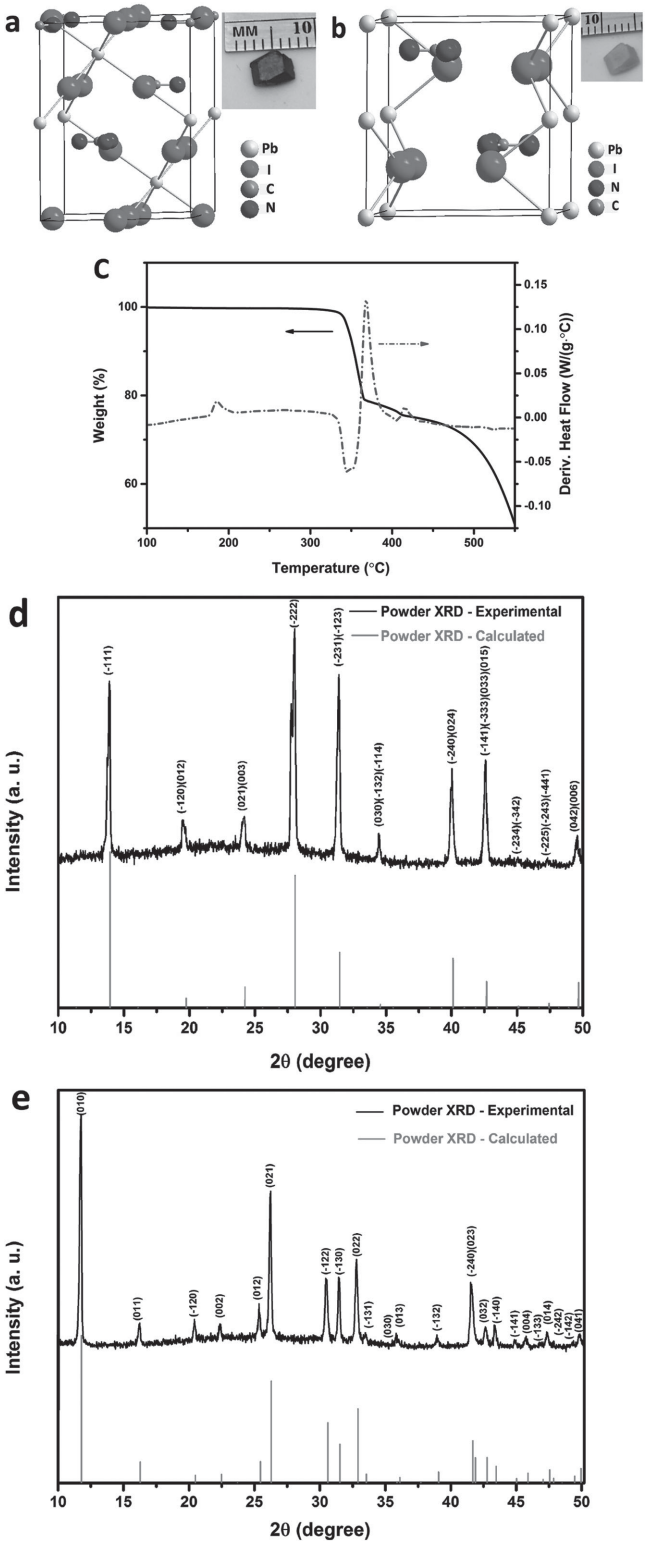

Figure 1. Crystal structures of a) α-phase and b) δ-phase single crystal $FAPbI_3$. The inset of (a) and (b) are images of α-phase and δ-phase single crystal, respectively. c) TGA-DSC curves of single crystal $FAPbI_3$. d) and e) are experimental and calculated powder XRD patterns of α-phase single crystal $FAPbI_3$ and δ-phase $FAPbI_3$, respectively.

Adv. Mater. **2016**,
DOI: 10.1002/adma.201505002

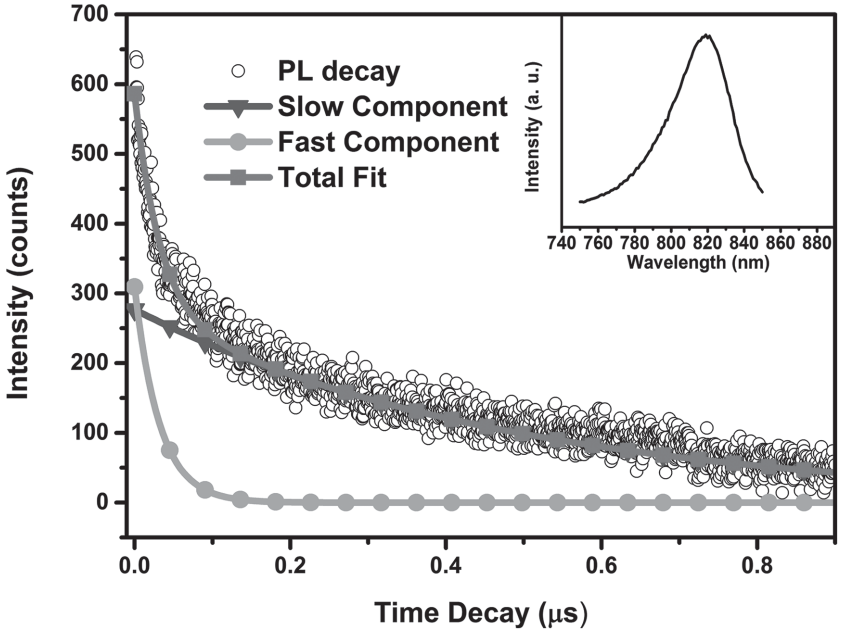

Figure 2. Decay traces of time-dependent PL on a α-phase single crystal $FAPbI_3$ at $\lambda = 820$ nm with the biexponential fitting showing a fast ($\tau_1 = 32$ ns, green) and a slow transient ($\tau_2 = 484$ ns, blue). The inset shows the emission PL peak of α-phase single crystal $FAPbI_3$.

633 nm. An emission peak of single crystal α-phase $FAPbI_3$ at 820 nm was observed (the inset of **Figure 2**). In a 300 nm thick $FAPbI_3$ thin film, the emission peak occurred at 805 nm (inset of Figure S3, Supporting Information), resulting in a blueshift of the emission peak. The shift of absorption edge is also observed in the UV–vis spectra shown in Figure S4 (Supporting Information). This means that the single crystal structure has a lower bandgap than that of the thin film. Single crystals are predominantly free of grain boundaries or structural defects, which could reduce the localized defect states. Thus the redshift of single crystal $FAPbI_3$ PL can be related to the higher material quality than thin film $FAPbI_3$. This indicates that the crystal quality in the current $FAPbI_3$ thin film, and the resulting performance of $FAPbI_3$-based solar cells, still have room to improve. The larger bandgap of single crystal δ-$FAPbI_3$ was confirmed by using a UV–vis absorption and PL spectrum as shown in Figure S5 (Supporting Information).

Carrier lifetime (τ) of single crystal $FAPbI_3$ was investigated by using time-dependent PL (TDPL) measurement. Transient fluorescent decay for the peak emission occurred from the photoexcitation at 820 nm as shown in Figure 2. The two-exponential decay showed fast (τ_1 = 32 ns) and slow (τ_2 = 484 ns) carrier lifetimes of the single crystal. The shorter lifetime originates from the high trap density related to the crystal surface conditions, and the longer lifetime represents the carrier transportation in bulk crystal having fewer defects.[23,33] The single crystal lifetime is much longer than that of the thin film ($\tau_1 = 29$ ns and $\tau_2 = 227$ ns, Figure S3, Supporting Information), which indicates that the single crystal $FAPbI_3$ has much lower quantity of defects. It is expected that enhanced crystallinity of the $FAPbI_3$ would contribute to improvement of the power conversion efficiency of the thin film solar cell. Compared to single crystal $MAPbI_3$, $FAPbI_3$ has relatively shorter carrier lifetime,[22,23] which might be related to the fact that pure $FAPbI_3$-based solar cells have relatively low efficiency below 15%.[34]

Current–voltage (I–V) measurement was performed using the single crystal $FAPbI_3$ deposited two indium electrodes on opposite sides in the dark (**Figure 3**). Ohmic and quadratic regions were clearly separated at a bias voltage of 33 V. The result fits well with the Mott's Space charge-limited current (SCLC) theory, i.e., beyond the bias voltage of 33 V, the current follows Mott–Gurney's square law

$$J_D = \frac{9\varepsilon\varepsilon_0 \mu V_b^2}{8L^3} \quad (1)$$

where J_D, ε, ε_0, μ, V_b, and L are the dark current, the relative dielectric constant, the vacuum permittivity, the mobility of single crystal $FAPbI_3$, applied voltage, and the thickness of the single crystal, respectively. We can generally estimate the carrier mobility to be 4.4 $cm^2\ V^{-1}\ s^{-1}$ from quadratic region, using relative dielectric constant ε = 46.9 measured in our lab. Time of flight (ToF) shown in Figure S6 (Supporting Information) was also used to measure the carrier mobility of 1.07 ± 0.25 $cm^2\ V^{-1}\ S^{-1}$ according to the equation $\mu = L^2/V\tau$, where μ, L, V, and τ are the mobility, the thickness, applied voltage, and the transit time of α-phase $FAPbI_3$ single crystal, respectively. This mobility value is smaller but of the same order of magnitude comparing to the result from SCLC measurement.

The applied voltage at the kink point of current increasing linearly and nonlinearly versus voltages is the trap-filled limit voltage (V_{TFL}), which is determined by the defect density[22,23]

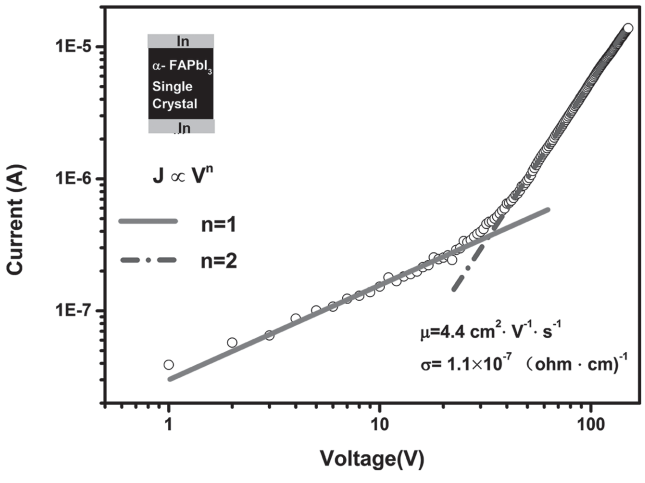

Figure 3. Dark current–voltage curve of α-phase single crystal $FAPbI_3$ for space charge limited current analysis.

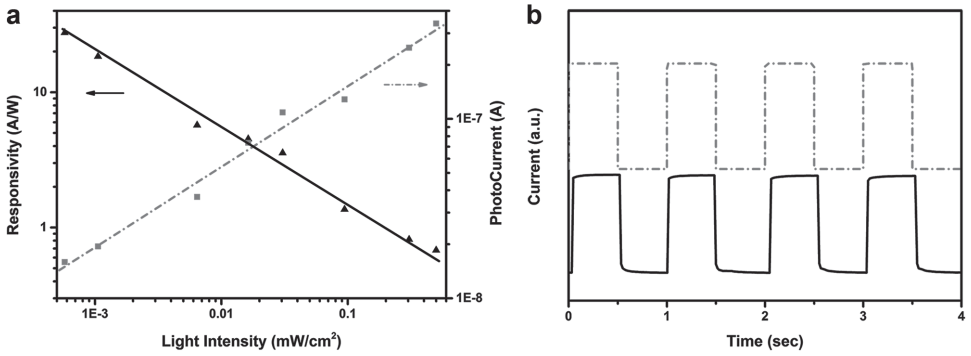

Figure 4. Device configuration and characteristics of the photodetector based on single crystal $FAPbI_3$. a) Photocurrent and photoresponsivity of devices for incident power densities. b) Transient photocurrent response at a pulse frequency of 1 Hz.

$$V_{TFL} = \frac{en_t L^2}{2\varepsilon\varepsilon_0} \quad (2)$$

where e is elementary charge, n_t is defect density, L is the thickness of $FAPbI_3$ material, ε_0 is vacuum permittivity, and ε is relative dielectric constant. The defect density of α-phase $FAPbI_3$ single crystal is 6.2×10^{11} cm^{-3}, which is an order of magnitude higher than that of single crystal $MAPbI_3$.[23]

Using the linear region data, the conductivity and carrier concentration of single crystal $FAPbI_3$ can be calculated to be $\sigma = 1.1 \times 10^{-7}$ $(\Omega\ \text{cm})^{-1}$ and $n = 1.5 \times 10^{11}$ cm^{-3}, respectively. Interestingly, the conductivity of the single crystal $FAPbI_3$ is an order of magnitude higher than that of single crystal $MAPbI_3$ ($\sigma = 1 \times 10^{-8}$ $(\Omega\ \text{cm})^{-1}$),[23] which is mainly attributed to the higher carrier concentration. The higher carrier concentration could be related to lower bandgap for $FAPbI_3$, possibly the difference in crystal structure, the electronic structure, and defect density, which clearly deserves further study.

The mobilities, conductivities, carrier concentrations, and defect density of δ-phase $FAPbI_3$ single crystal are $\mu = 0.179$ cm^2 V^{-1} S^{-1}, $\sigma = 8.9 \times 10^{-9}$ $(\Omega\ \text{cm})^{-1}$, $n = 3.1 \times 10^{11}$ cm^{-3}, and $n_t = 2.6 \times 10^{12}$ cm^{-3}, respectively, which are also calculated by SCLC theory shown in Figure S7 (Supporting Information). The conductivity decreases compare to α-phase $FAPbI_3$ single crystal could be attributed to the higher bandgap and defect density than α-phase $FAPbI_3$ single crystal. Moreover, the conductivity of α-phase $FAPbI_3$ thin film and single crystal are similar, which is consistent to $MAPbI_3$ result.[35] However, the mobility (1.1×10^{-3} cm^2 V^{-1} S^{-1}) decreases and defect density (1.3×10^{16} cm^{-3}) increases comparing to its single crystal as shown in Figure S8 (Supporting Information).

Combining the Einstein relation, $D = \mu K_B T/q$ and the definition of diffusion length $L = \sqrt{D\tau}$, where D is the diffusion constant, K_B is Boltzmann's constant, T is the absolute temperature, and q is the elementary charge, we can calculated the carrier diffusion length of α-phase $FAPbI_3$. The short and long diffusion lengths calculated from the short and long lifetimes were 0.5 μm and 2.2 μm, respectively. Using a similar measurement method, Bakr et al. observed similar short (2 μm) and long (8 μm) components in diffusion length for the $MAPbI_3$ single crystal. Adopting the methodology of this group, here the long and short diffusion lengths were assigned to the bulk and surface components of $FAPbI_3$ single crystals, respectively. Since both $MAPbI_3$ and $FAPbI_3$ have relatively long diffusion length, and $FAPbI_3$ has a broader light absorption ability, it is reasonable to expect that a mixed perovskite absorption layer such as (FA/MA)PbX_3 (X can be a pure or combination of halides—Cl, Br, and I) can improve solar cell performance as reported.[36]

The excellent material properties such as the large light absorption coefficient, high carrier mobility, long carrier lifetime, and long diffusion length of the $FAPbI_3$ single crystal strongly suggest that it is a suitable material for photodetector. Therefore, a photoconductive type photodetector based on single crystal $FAPbI_3$ was fabricated to prove the concept. The schematic illustration of the photodetector is shown in Figure S9 (Supporting Information). The devices were evaluated under the power intensity and the wavelength variations. **Figure 4**a shows a plotted linear response of single crystal $FAPbI_3$-based photodetectors within the incident light power density range from 5×10^{-4} to 5×10^{-1} mW cm^{-2} at 380 nm (incident photon flux density range from 9.56×10^{11} to 9.56×10^{14} number s^{-1} cm^{-2}) under 0.1 V bias. The photoresponsivity decreased linearly from 27.57 to 0.68 A W^{-1} when the light intensity increased, which is attributed to the enhanced charge recombination under higher light intensity.

Figure 4b represents the photoswitching of the devices at a frequency of 1 Hz, a wavelength of 380 nm, and a light intensity of 1 mW cm^{-2}. The photocurrent rapidly increased to a high level and recovered to the dark state. The rise time (t_r) of the device (from 10% to 90% of the saturated value) is 17 ms, whereas the fall-time (t_f) (from 90% to 10% peak value) is 21 ms.[37] The rise and decay dynamic response of this photodetector could also be described by Equations (3) and (4), respectively[38,39]

$$I_{light} = I_{dark} + A\left[\exp\left(t/T_1\right)\right] + B\left[\exp\left(t/T_2\right)\right] \quad (3)$$

$$I_{light} = I_{dark} + A\left[\exp\left(-t/T_3\right)\right] + B\left[\exp\left(-t/T_4\right)\right] \quad (4)$$

where I_{dark} is the dark current, A and B are the scaling constants, t is the time when the light was turned on or off, and T_1, T_2, T_3, and T_4 are the time constants. T_1 and T_3 should be related to the carrier generation and recombination processes in the crystal, and T_2 and T_4 should be mainly related to carrier

Adv. Mater. 2016,
DOI: 10.1002/adma.201505002

trapping and release processes. By fitting the experimental data with the two equations, the rise and fall times were calculated to be 12.4 and 17.2 ms, respectively (shown in Figure S10, Supporting Information). Thus the two approaches agree well, while the second one gives a more physical insight into the device. This response of the device is faster than perovskite–graphene hybrid photodetectors and ZnO/Au nanoparticle transparent photodetectors,[40,41] which reported values of larger than 87 ms and 10 s. The result is also comparable to the state-of-the-art photoconductor results reported in an organic planar-type photodetectors (≥10 ms) and nanocrystals-type photoconductivity photodetectors (≈20 ms).[42,43]

One of the figure-of-merit factors in photodetectors, noise equivalent power (NEP), is a key parameter defining the device sensitivity. It can be expressed by the equation below

$$\mathrm{NEP}=\left(Af\right)^{1/2}/D^{*}=i_{n}/R \tag{5}$$

where A is the effective area of the detector, f is the electrical bandwidth, D^* is the detectivity, i_n is the noise current, and R is responsivity.[44] A smaller NEP value corresponds to higher photosensitivity. To calculate NEP, we measured the noise current using a lock-in amplifier. Interestingly, the noise current of the devices is only 0.13 pA $Hz^{-1/2}$ at 1 Hz. The calculated NEP of the devices is $\approx 2.6 \times 10^{-14}$ W at 380 nm, which is better than the perovskite photodiode type photodetector.[44] The very small noise current and low NEP therefore lays a solid foundation for constructing highly sensitive photodetectors.

In summary, a large 5 mm sized single crystal $FAPbI_3$ has been successfully grown using a novel liquid-based crystallization method. The single crystal $FAPbI_3$ demonstrated a δ-phase to α-phase transition with a color change from yellow to black when heated to 185 °C within ≈2 min. The crystal structures of the two phases were identified and the PL emission peak of the α-phase $FAPbI_3$ (820 nm) shows clear redshift compared to the $FAPbI_3$ thin film (805 nm). The $FAPbI_3$ single crystal shows a long carrier lifetime of 484 ns, a high carrier mobility of 4.4 $cm^2\ V^{-1}\ s^{-1}$, and even more interestingly a conductivity of $1.1 \times 10^{-7}(\Omega\ cm)^{-1}$, which is approximately one order of magnitude higher than that of the $MAPbI_3$ single crystal. Finally, high performance photoconductivity type photodetectors were successfully demonstrated using the single crystal $FAPbI_3$, which paves the way for future optoelectronic device applications. The study of underlying properties of single crystal $FAPbI_3$ is important for improving the perovskite solar cell technology since $FAPbI_3$ has a broad absorption spectrum and good electronic properties.

Experimental Section

Chemicals and Reagents: Lead (II) acetate trihydrate ($Pb(ac)_2{\cdot}3H_2O$, 99%), fomamidine acetate salt (FAac, 99%), lead iodide (PbI_2, 99.999%), hydriodic acid (HI) (57% w/w aq. soln., stab with 1.5% hypophosphorous acid), and gamma-butyrolactone (GBL, 99%) were purchased from Sigma-Aldrich. Formamidinium iodide (FAI) was purchased from Dyesol Limited (Australia). All reagents and solvents were used as received without any further purification.

Synthesis of Seed Crystal of $FAPbI_3$: 2.5 g $Pb(ac)_2{\cdot}3H_2O$ was fully dissolved in 15 mL of HI in a 100 mL flask which was put into a 105 °C oil bath to heat up the mixed acid solution. A blend solution of 1.5 mL HI solution and 0.7 g of FAac was added to the mixed acid solution. Then the temperature of mixed solution was decreased to 70 °C and kept for 6 h for the precipitation of seed crystal $FAPbI_3$ (≈1 mm in size). The seed crystals were washed by diethyl ether and dried in vacuum.

Synthesis of Single Crystal $FAPbI_3$: At the beginning, 1.0 M solution containing PbI_2 and FAI (1:1) was dissolved in GBL at 60 °C overnight. Then, the solutions were filtered using polytetrafluoroethylene filter with 0.2 μm pore size. By placing the seed into this GBL solution in oil bath ≈100–105 °C for 3 h, the seed crystals grow into a large one. A larger crystal was formed by using this large crystal as the new seed put into a fresh precursor again. By repeating the above process three times, a large single crystal $FAPbI_3$ was synthesized.

Synthesis of $FAPbI_3$ Thin Films and Permittivity Measurement: 450 mg of PbI_2 was dissolved in 1 mL dimethylformamide and then was spin-coated at indium-tin-oxide substrates at 2500 rpm for 30 s. Then, FAI (dissolved in 2-propanol) was spin-coated on the top of dried PbI_2 layer at room temperature at 3000 rpm for 30 s in the dry air. All films were annealed in the air at 150 °C for desired time. Impedance spectroscopy of parallel plate capacitor from 10^4 to 10^6 Hz was used to measure permittivity of the $FAPbI_3$.

The permittivity was calculated from the following equation[45]

$$\varepsilon_r(f)=\frac{d}{A\varepsilon_0}\frac{-1}{2\pi f\ \mathrm{Im}(Z)} \tag{6}$$

where ε_0 is the permittivity of vacuum, A is the capacitor area, and d is the distance between the two electrodes.

Measurement and Characterization: TGA-DSC was performed on a TA SDT-Q600. The crystal structures of the nanocrystals were characterized by D8 Focus X-ray diffraction and Raman spectra (Renishaw inVia Raman spectrometer) with an incident laser of 514.5 nm. Steady-state PL of α-phase single crystal was measured using Horiba Jobin Yvon system with an excitation of 640 nm, and the δ-phase single crystal PL spectrum is measured using a NKT SuperK Extreme lase with an excitation of 475 nm and New Focus Si fW detector. TDPL was acquired using the time-correlated single-photon counting technique (Picoharp 300), and the excitation was provided by using a picosecond diode laser at the wavelength of 640 nm with a repetition frequency of 1 MHz (PDL 800B). The absorption spectrum was measured using U-4100 Hitachi UV–vis spectrophotometer. All current–voltage measurements were carried out by Agilent 4155C semiconductor parameter analyzer. ToF measurement was conducted by illuminating the devices with Laser Innovations DUO-220 dye laser. SR-570 current preamplifier with a bandwidth of 1 MHz was used to amplify the weak photocurrent, which recorded using a Tektronix DPO 4104 Digital Phosphor Oscilloscope. The Tektronix AFG 3252 function generator was used for frequency response measurements. Newport Model 1830-C was employed to gauge actual light intensity.

Supporting Information

Supporting Information is available from the Wiley Online Library or from the author.

Acknowledgements

Q.H., S.-H.B., and P.S. contributed equally to this work. This work was financially supported by a grant from the National Science Foundation (Grant No. ECCS-1509955, Program Director: Dr. Nadia El-Masry and ECCS- 1202231, Program Director: Dr. Radhakishan Baheti), Air Force Office of Scientific Research (Grant No. FA9550-15-1-0333, Program Manager: Dr. Charles Lee), Innovation Program of Shanghai Municipal Education Commission (No. 14YZ079), and Shanghai Municipal Natural Science Foundation (14ZR1430500). The authors sincerely acknowledge

Nicholas De Marco and Onur Sahin for their help with English editing and Dr. Baolai Liang for his help on δ-phase $FAPbI_3$ single crystal PL measurements. Qifeng Han appreciates Yingwei Li's help on XRD analysis.

Received: October 11, 2015
Revised: December 2, 2015
Published online:

[1] A. Kojima, I. Masashi, T. Kenjiro, M. Tsutomu, *Chem. Lett.* **2012**, *41*, 397.
[2] Q. Chen, N. D. Marco, Y. Yang, T. B. Song, C. C. Chen, H. Zhao, Z. Hong, H. Zhou, Y. Yang, *Nano Today* **2015**, *10*, 355.
[3] C. Wehrenfennig, G. E. Eperon, M. B. Johnston, H. J. Snaith, L. M. Herz, *Adv. Mater.* **2014**, *26*, 1584.
[4] H. Oga, A. Saeki, Y. Ogomi, S. Hayase, S. Seki, *J. Am. Chem. Soc.* **2014**, *136*, 13818.
[5] W. Zhang, M. Saliba, D. Moore, S. Pathak, M. T. Hörantner, T. Stergiopoulos, S. D. Stranks, G. E. Eperon, J. A. Alexander-Webber, A. Abate, A. Sadhanala, S. Yao, Y. Chen, R. H. Friend, L. A. Estroff, U. Wiesner, H. J. Snaith, *Nat. Commun.* **2015**, *6*, 6142.
[6] S. Kazim, M. K. Nazeeruddin, M. Grätzel, S. Ahmad, *Angew. Chem. Int. Ed.* **2014**, *53*, 2812.
[7] M. Liu, M. B. Johnston, H. J. Snaith, *Nature* **2013**, *501*, 395.
[8] J. Burschka, N. Pellet, S. J. Moon, R. Humphry-Baker, P. Gao, M. K. Nazeeruddin, M. Grätzel, *Nature* **2013**, *499*, 316.
[9] H. J. Snaith, *J. Phys. Chem. Lett.* **2013**, *21*, 3623.
[10] N. G. Park, *Mater. Today* **2015**, *18*, 65.
[11] M. Gratzel, *Nat. Mater.* **2014**, *13*, 838.
[12] M. A. Green, A. Ho-Baillie, H. J. Snaith, *Nat. Photonics* **2014**, *8*, 506.
[13] H. Zhou, Q. Chen, G. Li, S. Luo, T. B. Song, H. S. Duan, Z. Hong, J. You, Y. Liu, Y. Yang, *Science* **2015**, *345*, 542.
[14] N. Ahn, D. Y. Son, I. H. Jang, S. M. Kang, M. Choi, N. G. Park, *J. Am. Chem. Soc.* **2015**, *137*, 8696.
[15] S. Pang, H. Hu, J. Zhang, S. Lv, Y. Yu, F. Wei, T. Qin, H. Xu, Z. Liu, G. Cui, *Chem. Mater.* **2014**, *26*, 1485.
[16] G. E. Eperon, S. D. Stranks, C. Menelaou, M. B. Johnston, L. M. Herz, H. J. Snaith, *Energy Environ. Sci.* **2014**, *7*, 982.
[17] T. M. Koh, K. Fu, Y. Fang, S. Chen, T. C. Sum, N. Mathews, S. G. Mhaisalkar, P. P. Boix, T. Baikie, *J. Phys. Chem. C* **2013**, *118*, 16458.
[18] N. Pellet, P. Gao, G. Gregori, T. Y. Yang, M. K. Nazeeruddin, J. Maier, M. Grätzel, *Angew. Chem. Int. Ed.* **2014**, *53*, 3151.
[19] W. S. Yang, J. H. Noh, J. J. Nam, Y. C. Kim, S. Ryu, J. Seo, S. I. Seok, *Science* **2015**, *348*, 1234.
[20] S. Pang, H. Hu, J. Zhang, S. Lv, Y. Yu, F. Wei, T. Qin, H. Xu, Z. Liu, G. Cui, *Chem. Mater.* **2014**, *26*, 1485.
[21] A. Binek, F. C. Hanusch, P. Docampo, T. Bein, *J. Phys. Chem. Lett.* **2015**, *6*, 1249.
[22] Q. Dong, Y. Fang, Y. Shao, P. Mulligan, J. Qiu, L. Cao, J. Huang, *Science* **2015**, *347*, 967.
[23] D. Shi, V. Adinolfi, R. Comin, M. Yuan, E. Alarousu, A. Buin, Y. Chen, S. Hoogland, A. Rothenberger, K. Katsiev, Y. Losovyj, X. Zhang, P. Dowben, O. F. Mohammed, E. H. Sargent, O. M. Bakr, *Science* **2015**, *347*, 519.
[24] J. Su, D. P. Chen, C. T. Lin, *J. Cryst. Growth* **2015**, *422*, 75.
[25] Y. Dang, Y. Liu, Y. Sun, D. Yuan, X. Liu, W. Lu, G. Liu, H. Xia, X. Tao, *CrystEngComm* **2015**, *17*, 665.
[26] M. I. Saidaminov, A. L. Abdelhady, B. Murali, E. Alarousu, V. M. Burlakov, W. Peng, I. Dursun, L. Wang, Y. He, G. Maculan, A. Goriely, T. Wu, O. F. Mohammed, O. M. Bakr, *Nat. Commun.* **2015**, *6*, 7586.
[27] Y. Liu, Z. Yang, D. Cui, X. Ren, J. Sun, X. Liu, J. Zhang, Q. Wei, H. Fan, F. Yu, X. Zhang, C. Zhao, S. Liu, *Adv. Mater.* **2015**, *27*, 5176.
[28] C. C. Stoumpos, C. D. Malliakas, M. G. Kanatzidis, *Inorg. Chem.* **2013**, *52*, 9019.
[29] M. I. Saidaminov, A. L. Abdelhady, G. Maculana, O. M. Bakr, *Chem. Commun.* **2015**, *51*, 17658.
[30] L. Q. Fan, J. H. Wu, *Acta Crystallogr., Sect. E* **2007**, *63*, i189.
[31] R. Gottesman, L. Gouda, B. S. Kalanoor, E. Haltzi, S. Tirosh, E. Rosh-Hodesh, Y. Tischler, A. Zaban, *J. Phys. Chem. Lett.* **2015**, *6*, 2332.
[32] C. Quarti, G. Grancini, E. Mosconi, P. Bruno, J. M. Ball, M. M. Lee, H. J. Snaith, A. Petrozza, F. De Angelis, *J. Phys. Chem. Lett.* **2014**, *5*, 279.
[33] T. S. Horfinyi, T. Pavelka, P. Tutto, *Appl. Surf. Sci.* **1993**, *63*, 306.
[34] G. E. Eperon, S. D. Stranks, C. Menelaou, M. B. Johnston, L. M. Herz, H. J. Snaith, *Energy Environ. Sci.* **2014**, *7*, 982.
[35] K. Sveinbjrnsson, K. Aitola, X. Zhang, M. Pazoki, A. Hagfeldt, G. Boschloo, E. M. J. Johansson, *J. Phys. Chem. Lett.* **2015**, *6*, 4259.
[36] N. J. Jeon, J. H. Noh, W. S. Yang, Y. C. Kim, S. Ryu, J. Seo, S. I. Seok, *Nature* **2014**, *517*, 476.
[37] J. M. Liu, *Photonic Devices*, Cambridge University Press, Cambridge **2005**.
[38] B. Chitara, L. Panchakarla, S. Krupanidhi, C. Rao, *Adv. Mater.* **2011**, *23*, 5419.
[39] Z. Sun, Z. Liu, J. Li, G. A. Tai, S. P. Lau, F. Yan, *Adv. Mater.* **2012**, *24*, 5878.
[40] Y. Lee, J. Kwon, E. Hwang, C. H. Ra, W. J. Yoo, J. H. Ahn, J. H. Park, J. H. Cho, *Adv. Mater.* **2015**, *27*, 41.
[41] Z. Jin, L. Gao, Q. Zhou, J. Wang, *Sci. Rep.* **2014**, *4*, 4268.
[42] B. Mukherjee, M. Mukherjee, Y. Choi, S. Pyo, *J. Phys. Chem. C* **2009**, *113*, 18870.
[43] S. Hinds, L. Levina, E. J. D. Klem, G. Konstantatos, V. Sukhovatkin, E. H. Sargent, *Adv. Mater.* **2008**, *20*, 1.
[44] L. Dou, Y. Yang, J. You, Z. Hong, W. H. Chang, G. Li, Y. Yang, *Nat. Commun.* **2014**, *5*, 5404.
[45] S. Y. Leblebici, T. L. Chen, P. Olalde-Velasco, W. Yang, B Ma, *ACS Appl. Mater. Interfaces* **2013**, *5*, 10105.